# Triplet State Excitation of Alkali Molecules on Helium Droplets: Experiments and Theory†

**Gerald Auböck,* Johann Nagl, Carlo Callegari, and Wolfgang E. Ernst**

*Institute of Experimental Physics, TU Graz, Petersgasse 16, 8010 Graz, Austria, EU*

*Received: February 1, 2007; In Final Form: April 3, 2007*

In this paper, we discuss the electronic structure of alkali dimer molecules in $^3\Pi_g$ states on the surface of a helium droplet. The perturbation due to the droplet will in general not satisfy rotational symmetry around the internuclear axis of the diatom and thus, in addition to a broadening and blue shift, will cause a splitting of electronic levels that are degenerate in the free molecules. We propose a model based on general symmetry arguments and on a small number of physically reasonable parameters. We demonstrate that such a model accounts for the essential features of laser-induced fluorescence (LIF) and magnetic circular dichroism (MCD) spectra of the $(1)^3\Pi_g-a^3\Sigma_u^+$ transition of $Rb_2$ and $K_2$. Furthermore the MCD spectra, analyzed according to the approach of Langford and Williamson [*J. Phys. Chem. A* **1998**, *102*, 2415], allow a determination of the populations of Zeeman sublevels in the ground state and thus a measurement of the surface temperature of the droplet. The latter agrees with the accepted temperature, 0.37 K, measured in the interior of a droplet.

## I. Introduction

Helium nanodroplets are capturing the attention of a broad, steadily growing, community (see refs 1−5 for recent reviews). A strong drive came from the experimental confirmation of properties that are both of great interest and unique to He droplets. The droplets equilibrate by evaporative cooling[6] to the very low temperature of 0.37 K (ref 7). They do, however, remain liquid (even in the presence of a dopant) and are in fact superfluid.[8] For the brief time-of-flight through a typical vacuum chamber ($10^{-3}$ s), each droplet constitutes an isolated sample of the weakest existing solvent, which can be loaded almost at will with atomic and molecular dopants. Dopants move rather unhindered within a He droplet, as compared with other matrices, and the weak perturbation eases spectroscopic assignment.

Helium nanodroplets are of great interest for the study of superfluidity on the atomic scale,[3] as manifested in the coupling and relaxation (or lack thereof) of electronic,[8,9] vibrational,[10] rotational,[11,12] and spin[13−15] degrees of freedom. Ongoing "textbook" experiments are successfully building doped clusters "from the bottom up" (currently up to 72 He atoms).[16] The size-resolved spectra of these clusters are truly bridging the gap between the single atom and bulk matter. Larger droplets are routinely used as cryostats to embed and cool to the temperature of the droplet the most diverse species, such as atoms, small and large[17] stable molecules, and radicals,[18] as well as to assemble weakly bound complexes,[19−21] possibly metastable against vibrational[22] or electronic excitation.[23,24] Helium droplets have also found a niche in the cold (<1 K) molecule community: [25] despite being in the high millikelvin range, they are useful to produce and study molecules and processes of interest at lower temperature, such as alkali pair potentials, trimers, collisions, and molecule deceleration.

Structural information has come for the most part through rovibrational spectroscopy, starting from the early experiments[7,26] and continuing with the extensive work of the late Roger E. Miller and his collaborators.[1,27]

Electronic spectroscopy has provided information about potential energy surfaces of difficult-to-make species.[23,28−32] We note the high-resolution emission spectra of species released from the droplet after excitation.[29,33,34]

Electronic excitations couple well to the helium motion and have been exploited to investigate helium excitations.[35] Dispersed fluorescence,[36] time-correlated photon counting,[37] multiphoton ionization,[38] and femtosecond pump−probe methods[39−42] have all been successfully used to look into the dynamics of excited systems. Electronic excitation has also been a means to initiate simple chemical reactions in van der Waals complexes formed in or on the droplet.[23,24]

In all these applications, spectral assignment is, as mentioned, eased by the weakness of the helium−host interaction. For chromophores whose gas-phase spectrum is known, it is often sufficient to treat the droplet as a small perturbation. Many spectra have been assigned and satisfactorily modeled (often with vibrational resolution)[43] by simply shifting the corresponding gas-phase spectra and empirically allowing for a modest line broadening. The extent of the shift has been used to decide on the surface-versus-solvated state of atomic dopants.[44,45]

Broadening rather than, say, scrambling of levels is normally the factor limiting the information that can be extracted from a spectrum. In some favorable cases, electronic transitions are rather sharp, and one or more zero-phonon lines are observed. Multiple zero-phonon lines are assigned to different conformers[46] or to elementary excitations of the liquid.[35,46−51]

Some systems are special in that interaction with the helium environment decreases the symmetry of the chromophore and thus may cause degenerate levels to split. From these, one gains additional information on the chromophore−droplet interaction. Which substate is accessed may also have a strong influence on the dynamics of the system.[36,52−54] Thus, the photon energy of the exciting laser provides a useful control handle for the experimenter. Some of these degeneracies are spin-related[15,34,36] and make the system interesting for magnetic studies, light polarization effects, and optical pumping.

Triplet alkali dimers are one such system; the structure of the electronic spectra involving a $^3\Pi$ state has escaped assign-

† Part of the "Roger E. Miller Memorial Issue".

10.1021/jp070891y CCC: $37.00 
Published on Web 06/07/2007

ment so far. In this paper, we present measurements of laser-induced fluorescence (LIF) and magnetic circular dichroism (MCD) spectra of the $(1)^3\Pi \leftarrow a^3\Sigma$ band in alkali dimers formed on the surface of helium nanodroplets. We focus in particular on the $Rb_2$ molecule, whose electronic structure in the $(1)^3\Pi_g$ state—as perturbed by the helium droplet—we discuss in detail. We develop a model based on general symmetry arguments and on a small number of physically reasonable parameters, which is able to accurately reproduce both the LIF and MCD spectra. The model also reproduces, somewhat less accurately, the corresponding $K_2$ spectra. Further analysis of the $Rb_2$ MCD spectra with standard methods allows us to conclude that the valence-electron spins of the molecule have thermalized to the temperature of the droplet. Alkali dimers thus provide the first instance of a "surface thermometer".

## II. Experimental Procedures

Our experimental setup without magnetic field is described in detail in ref 34. In brief, helium droplets are produced in a supersonic expansion of grade 6 helium through a 5 $\mu$m nozzle, with typical stagnation pressure ~60 bar and nozzle temperature, $T_n \approx 14$ K, corresponding to a mean size of some 10 000 He atoms. The skimmed beam passes through a pickup cell filled with rubidium metal and heated to 140 °C. Under these conditions, the likelihood is high that two Rb atoms per droplet will be picked up. These in turn form a $Rb_2$ molecule on the droplet in either the $X^1\Sigma_g^+$ state (true ground state) or the $a^3\Sigma_u^+$ state (lowest triplet state). Because of the anticorrelation between formation energy and survival probability, a molecule in the weakly bound triplet state is much more likely to remain on the droplet than one in the singlet state, and the beam becomes correspondingly enriched.[43] Because these two states are not observed to interconvert on a He droplet, and because the singlet state does not further enter our analysis, we will refer to the $a^3\Sigma_u^+$ as the ground state, as if singlet $Rb_2$ and triplet $Rb_2$ were chemically different species.

The beam is crossed at right angle by the slightly focused output of a cw Ti:$Al_2O_3$ ring laser (Coherent 899-01, multiline operation). The lab reference frame is so defined: the supersonic and laser beams propagate along the positive $Y$ and $Z$ axis, respectively. The laser-induced fluorescence (LIF) is collected with a low-numerical-aperture lens system along the positive $X$ axis (vertical) and detected by a Peltier-cooled photomultiplier tube (Hamamatsu R943-02). The excitation region is immersed in a magnetic field $B\hat{Z}$ obtained with two NdFeB permanent magnets (grade N35, diameter 30 mm, gap 17 mm). Within the gap $B = 2.9$ kG. A hole (5 mm diam) is drilled in the center of each magnet for laser access.

The laser beam is sent into the experimental chamber through a set of two Al mirrors and a lens. Just before the entrance window, the beam is linearly polarized and passed through a Pockels cell capable of continuously changing the polarization state of the beam, without affecting its intensity, as a control voltage is varied from −2.5 to 0 kV ($\sigma^-$ to linear, $l$) or from 0 to +2.5 kV ($l$ to $\sigma^+$).

LIF and MCD spectra are measured simultaneously with the following in-phase detection scheme: to cancel the background due to scattered laser light, we chop the droplet beam at 22.7 Hz; we additionally modulate the polarization of the laser beam between $\sigma^+$ and l at half this frequency, phase-locked to it. This defines a four-step cycle, and the corresponding signals $s_1$, $s_2$, $s_3$, and $s_4$, accumulated in a homemade four-channel counter for 2 s. Within each step, the counters are gated for 20 ms, exactly one period of the line frequency, so as to cancel out possible interference; this gating time is intentionally shorter than the duration of each step (22 ms), so as to eliminate the counts at the modulation edges. The background-free LIF signals, unnormalized, are then $s_{\sigma^+} = s_1 - s_2$ and $s_l = s_3 - s_4$. In the following, we will refer to the spectrum for linearly polarized laser light as the LIF spectrum. The MCD signal, conceptually defined as $m = s_{\sigma^+} - s_{\sigma^-}$, is operationally given by $m = 2(s_{\sigma^+} - s_l)$. Measurements done with modulation between linear and $\sigma^-$ polarized light give identical results, thus confirming the validity of our operational definition, which exploits the fact that in the absence of power-saturation effects $s_l = (s_{\sigma^+} + s_{\sigma^-})/2$.

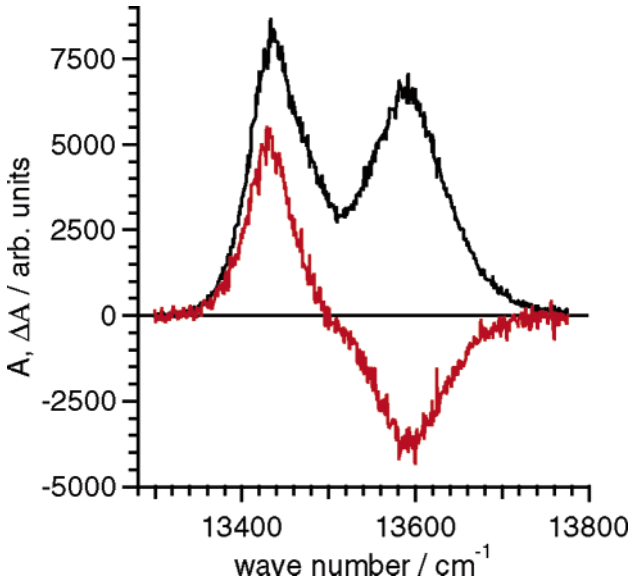


**Figure 1.** LIF (black) and MCD (red) spectrum of the $Rb_2$ $(1)^3\Pi_g - {}^3\Sigma_u^+$ transition on a He droplet. The spectra were recorded at a laser power of ~40 mW.

The resulting LIF and MCD spectra for the $(1)^3\Pi_g - a^3\Sigma_u^+$ transition are shown in Figure 1. They have been acquired far from power saturation and have been normalized to the power of the excitation laser. In the customary notation of MCD spectroscopy, we indicate these normalized spectra with $A$ and $\Delta A$, respectively.

## III. Discussion

We have already discussed in ref 34 many aspects of the LIF spectra under investigation, together with dispersed emission spectra of the same bands. Here we analyze in detail the perturbation of the excited electronic states induced by the He droplet.

We now define some quantities and notations that will be used below. The laboratory-fixed axes $X$, $Y$, and $Z$ have been given above; $x$, $y$, and $z$ are the axes of the molecule-fixed frame, $z$ being the molecular axis and the plane $xz$ being defined by the two Rb nuclei and the center of mass of the droplet. $\Lambda$ and $\Sigma$ denote the projections of the electronic and spin angular momenta, respectively, on the molecular axis. The total electronic angular momentum $\Omega$, with sign, is given by $\Lambda + \Sigma$. $A_\Pi = 70$ cm$^{-1}$ is the spin−orbit (SO) constant for $Rb_2$ in the $(1)^3\Pi_g$ state, which we deduced from dispersed emission spectra.[34] For $K_2$ in the corresponding state (see below), we set $A_\Pi$ equal to the atomic value, $A_P = 19$ cm$^{-1}$ ($^1/_3$ of the SO-splitting given in ref 55). Single-electron quantum numbers are indicated with $l$, $s$, $l_z$, and $s_z$ with obvious meanings. Molecular orbitals are indicated with lowercase greek letters as standard;

g and u subscripts indicate the symmetry under "molecule-fixed" inversion; ± superscripts indicate $\pi$ orbitals with $l_z = \pm 1$, *x* and *y* superscripts their symmetric and antisymmetric combinations for reflection through the *xz* plane; the presence or absence of a bar, respectively, indicates occupation by a $\beta$ or an $\alpha$ electron ($s_z = -1/2, +1/2$). Because for two electrons in a triplet state molecular orbitals are always singly occupied, we omit the occupation number. All spectra are calculated from $v = 0$, $j = 0$ of the electronic ground state.

**A. The $a^3\Sigma_u^+$ State.** We assume that the electronic wavefunction of the molecule in the ground state is not significantly modified by the weak interaction with the He droplet. The state is thus well described by a pure Hund's case (b) since spin−spin and higher-order spin−orbit coupling are small for this state [$V(^3\Sigma_1) - V(^3\Sigma_0) < 0.1$ cm$^{-1}$, ref 56] compared with the temperature of the droplet. For the sake of uniformity with the excited state, it is convenient to describe this state in a Hund's case (a) basis, $|^3\Sigma, \Lambda\Sigma\rangle$. In a magnetic field, the eigenstates of this term are determined by diagonalizing the Zeeman Hamiltonian in the $|^3\Sigma, \Lambda\Sigma\rangle$ basis as in ref 57.

**B. Electronic Structure of the $(1)^3\Pi_g$ State on a He Droplet.** Due to the large spin−orbit interaction of Rb, the $(1)^3\Pi_g$ term of the free $Rb_2$ molecule is split into three electronic states, according to the projection of the total electronic angular momentum on the internuclear axis ($\Omega = 0, \pm 1, \pm 2$). In the Franck−Condon-allowed region, the state is well in the limit of Hund's case (a): $\Lambda = \pm 1$ and $\Sigma = 0, \pm 1$ are good quantum numbers and $\Omega$ is redundantly given by their sum. We neglect for the moment the ± symmetrization of the $\Omega = 0$ state. The $|\Lambda\Sigma\Omega\rangle$ basis is convenient for inclusion of the perturbation induced by the He droplet. From the above discussion, based on a free-molecule picture, one would expect the transition to consist of three bands corresponding to the transitions $|\Omega'| \leftarrow |\Omega| = 0 \leftarrow 1, 1 \leftarrow 0, 2 \leftarrow 1$. Only two peaks are observed in our LIF spectrum (Figure 1). Practically the same structure has been observed for $K_2$ and KRb;[15,34,43,52] of particular relevance here is the fact that for both of them the peak separation[43,52] is too large to be accounted for by spin−orbit splitting alone. Similar structures observed for LiCs and NaCs (ref 30) are also at odds with the free-molecule picture, but $Cs_2$ (ref 54) is not.

Currently, little is known about the energetics and dynamics of an alkali dimer on a He droplet. Similarly, little is known about the He density distribution near the dimer, even in a static picture. This makes a quantitative calculation of the perturbation induced by the droplet challenging. As mentioned, experimental electronic spectra can often be well reproduced by adding a shift (to the blue, here) and a modest line broadening to the spectrum of the free molecule. Qualitatively, the observed blue shift is easily understood: If the electronic transition of the molecule is described as vertical (i.e., the positions of all nuclei, including the surrounding helium, do not change during the very short time of electronic excitation), the expansion of the molecular electronic wavefunction increases the overlap of the latter with the surrounding helium, which results in a repulsive interaction.

For an alkali molecule, sitting on the surface of the droplet, rotational symmetry around the internuclear axis is in general broken (except in the special case when the internuclear axis is perpendicular to the droplet surface). This can lead to a splitting of degenerate electronic states of the free molecule, which has been previously ignored. We will now develop a very simple semiempirical model, which captures the important features of the spectra reported here and may also apply to the other dimers mentioned above.

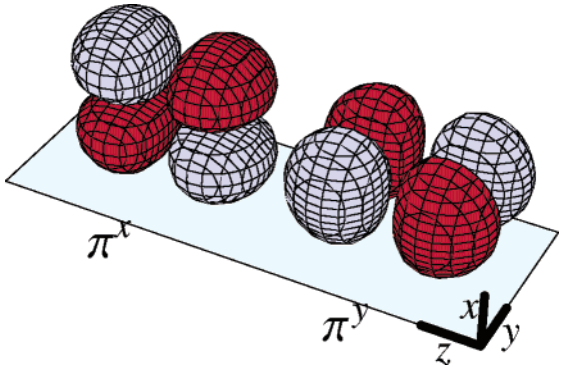


**Figure 2.** Pictorial representation of a $\pi_g^x$ and a $\pi_g^y$ molecular orbital on the surface of a He droplet. The *x*, *y*, *z* frame is molecule-fixed, with the *xz* plane perpendicular to the surface: shown here is the special case where the molecular axis lies parallel to the He surface.

The $(1)^3\Pi_g$ state of $Rb_2$ arises from a $(\sigma_g)(\pi_g^{\pm})$ occupation of molecular orbitals. Including spin, the properly symmetrized electronic wavefunctions $|\Lambda\ \Sigma\ \Omega\rangle$ are given by

$$
\begin{aligned}
|1\ 1\ 2\rangle &= (\sigma_g)(\pi_g^+) \\
|-1\ 1\ 0\rangle &= (\sigma_g)(\pi_g^-) \\
|1\ 0\ 1\rangle &= (1/\sqrt{2})[(\sigma_g)(\bar{\pi}_g^+) + (\bar{\sigma}_g)(\pi_g^+)] \\
|-1\ 0\ 1\rangle &= (1/\sqrt{2})[(\sigma_g\bar{\pi}_g^-) + (\bar{\sigma}_g)(\pi_g^-)] \\
|1\ -1\ 0\rangle &= (\bar{\sigma}_g)(\bar{\pi}_g^+) \\
|-1\ -1\ -2\rangle &= (\bar{\sigma}_g)(\bar{\pi}_g^-)
\end{aligned}
\qquad (1)
$$

These wavefunctions are eigenfunctions of the nonrelativistic electronic molecular Hamiltonian, $H_M$, plus the spin−orbit Hamiltonian, $\langle H_{SO}\rangle = A_\Pi \hat{L}_z \hat{S}_z$ ($= A_\Pi\Lambda\Sigma$ in our chosen basis). The corresponding energies are given by $V(^3\Pi_g) + A_\Pi(|\Omega| - 1)$. We use these wavefunctions as basis functions for the inclusion of a perturbation by the He droplet given by a Hamiltonian $H_D$.

Since He has no magnetic moment, it cannot act directly on the spin state of the electrons. It is thus sufficient to investigate the effect of the He surface on the electronic orbital wavefunctions $(\sigma_g)(\pi_g^{\pm})$. Since $H_D$ does not satisfy rotational symmetry around the internuclear axis, it will not be diagonal in the $(\sigma_g)(\pi_g^{\pm})$ basis. However, $H_D$ satisfies $\sigma_{xz}$ symmetry; that is, the electronic wavefunction must be either symmetric or antisymmetric for a reflection through the *xz*-plane, which contains the Rb nuclei and the center of mass of the droplet. This symmetry is satisfied by the wave functions $(\sigma_g)(\pi_g^x)$, symmetric, and $(\sigma_g)(\pi_g^y)$, antisymmetric. The energy (i.e., the diagonal matrix elements of $H_D$ in the new basis) for the two states will be different since each of them will yield a different overlap of the electron cloud with the He density distribution (see Figure 2). We call these matrix elements $V_x$ and $V_y$. They are difficult to calculate quantitatively since the exact He distribution is unknown. We include them as empirical parameters, whose value we show to be physically reasonable.

It is straightforward to transform $H_D$ to the basis given by eq 1 using the relation $(\sigma_g)(\pi_g^{\pm}) = (1/\sqrt{2})[(\sigma_g)(\pi_g^x) \pm$

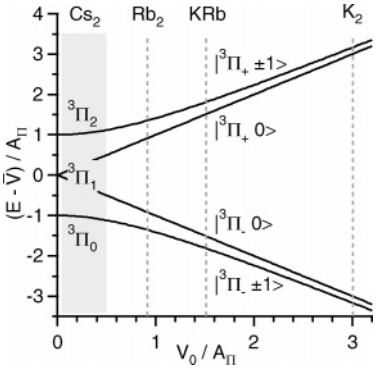


**Figure 3.** Correlation diagram for a $^3\Pi$ multiplet under the combined effect of a spin−orbit interaction $A_\Pi$ and a crystal field interaction $V_0$ as in eqs 2 and 3. Dashed vertical lines (shaded region, for $Cs_2$) indicate the collocation of various dimers according to the estimated value of the crystal field splitting, as given in Table 1.

$i(\sigma_g)(\pi_g^y)$]. The total Hamiltonian in the basis of eq 1 is then block diagonal and factors into three matrices

$$\begin{array}{lll} |\Lambda\,\Sigma\,\Omega\rangle & |-1\;0\;-1\rangle & |+1\;0\;+1\rangle \\ |-1\;0\;-1\rangle & \bar{V} & V_0 \\ |+1\;0\;+1\rangle & V_0 & \bar{V} \end{array} \tag{2}$$

and

$$\begin{array}{lll} |\Lambda\,\Sigma\,\Omega\rangle & |\pm1\;\pm1\;\pm2\rangle & |\pm1\;\mp1\;0\rangle \\ |\pm1\;\pm1\;\pm2\rangle & \bar{V}+A_\Pi & V_0 \\ |\pm1\;\mp1\;0\rangle & V_0 & \bar{V}-A_\Pi \end{array} \tag{3}$$

where $\bar{V} = (V_x + V_y)/2$ and $V_0 = (V_x - V_y)/2$.

This Hamiltonian has the same form as that used to analyze the MCD spectra of the NH radical by Langford and Williamson,[57] who give a detailed analysis of the resulting eigenstates, including Zeeman splitting in an external magnetic field. We note two typographical errors in their manuscript, namely, that equation numbering after eq 15 restarts at 11, and that $\delta_{M_\Lambda,M'_{\Lambda\pm1}}$ in the second instance of eq 11 should be $\delta_{M_\Lambda,M'_{\Lambda\pm2}}$. To retain consistency with their notation, we define $V_1 = (A_\Pi{}^2 + V_0{}^2)^{1/2}$ and use for $V_0$ the name "crystal field (CF) parameter". As in ref 57, the eigenvalues and eigenstates of the Hamiltonian at this level of perturbation are

$$E(^3\Pi_\pm\,\Sigma) = \pm(A_\Pi{}^2|\Sigma| + V_0{}^2)^{1/2} + \bar{V} \tag{4}$$

$$|^3\Pi_\pm\,0\rangle = 2^{-1/2}(|^3\Pi_1\,1\,0\rangle \pm |^3\Pi_1\,-1\,0\rangle) \tag{5}$$

$$|^3\Pi_+\,\pm1\rangle = \alpha|^3\Pi_0\,\mp1\,\pm1\rangle - \beta|^3\Pi_2\,\pm1\,\pm1\rangle \tag{6}$$

$$|^3\Pi_-\,\pm1\rangle = \beta|^3\Pi_0\,\mp1\,\pm1\rangle + \alpha|^3\Pi_2\,\pm1\,\pm1\rangle \tag{7}$$

with the mixing coefficients

$$\alpha = V_0/[V_0{}^2 + (V_1 + A_\Pi)^2]^{1/2} \tag{8}$$

$$\beta = V_0/[V_0{}^2 + (V_1 - A_\Pi)^2]^{1/2} \tag{9}$$

Note that Langford and Williamson do not have a $\bar{V}$ term, which they incorporate into a common term value $T_\Pi$ (the center of gravity of the band). A graph of $E - \bar{V}$ versus $V_0$ (both as nondimensional quantities, scaled to the strength of the spin−orbit coupling $A_\Pi$) is displayed in Figure 3.

One of the referees has suggested that the resulting level structure has a simple physical interpretation (implicit in our model): the electronic angular momentum in the excited state of $Rb_2$ is quenched by the interaction with the droplet; thus spin−orbit coupling is averaged out. Formalisms containing a "quenching Hamiltonian" term, for the analysis of rovibrational/electronic spectra of van der Waals complexes between an open-shell molecule and a closed-shell atom/molecule, have been developed by Mills et al.,[58] Fawzy and Hougen,[59] Dubernet et al.,[60] and Marshall and Lester.[61]

**C. Discussion of the LIF and MCD Spectra.** *1. The Analysis of Moments.* With the above Hamiltonian and the tools of ref 57, the populations of the Zeeman levels of the ground-state manifold can be determined from a moment analysis of the absorption spectrum. In the following, we assume that the LIF spectra of the band are faithful representations of the full absorption spectra. For alkali atoms and molecules on He droplets, it is considered a good assumption that the fluorescence quantum yield is 100%.[64] We indicate the power-normalized LIF and MCD spectra with $A(\tilde{\nu})$ and $\Delta A(\tilde{\nu})$, respectively, with $\tilde{\nu}$ the wavenumber of the exciting photon. This is consistent with the notation of ref 57 where, however, the photon energy $E = hc\tilde{\nu}$ is used instead.

The $n$th moments of the LIF and MCD spectrum are defined by

$$\mathbf{A}_n = \int(\tilde{\nu} - \bar{\tilde{\nu}})^n A(\tilde{\nu})\,\mathrm{d}\tilde{\nu} \tag{10}$$

$$\mathbf{M}_n = \int(\tilde{\nu} - \bar{\tilde{\nu}})^n \Delta A(\tilde{\nu})\,\mathrm{d}\tilde{\nu} \tag{11}$$

where $\bar{\tilde{\nu}}$ is defined by imposing $A_1 = 0$; note that, apart from the integration variable, our integrands differ from those of ref 57 by a factor $E$ (consistent with the fact that in their case $A$ and $\Delta A$ are intensities and in our case are photon counts).

The populations $P_1$, $P_2$, and $P_3$ of the Zeeman sublevels of the ground state (defined as in ref 57) are related to the experimental moments by

$$\begin{aligned} M_1/A_0 &= \mu_B B - A_\Pi(P_1 - P_3) \\ &= \mu_B B - \frac{2A_\Pi \sinh(g_e\mu_B B/k_B T)}{1 + 2\cosh(g_e\mu_B B/k_B T)} \end{aligned} \tag{12}$$

where $g_e \approx 2$ is the electron $g$-factor, $\mu_B$ the Bohr magneton, and $k_B$ the Boltzmann constant. The first line in eq 12 is the general case; the second assumes thermal equilibrium of the spins at a temperature $T$.

From our spectra and eqs 10 and 11, we obtain $M_1/A_0 = -45\ \mathrm{cm}^{-1}$; from eq 12 at $T = 0.37$ K (the inner temperature of a He droplet), we get $M_1/A_0 = -42\ \mathrm{cm}^{-1}$. We conclude from this good agreement, as we did for $K_2$,[15] that the population of Zeeman sublevels has reached thermal equilibrium with the He droplet. We note that the surface temperature of a droplet has never been measured. We cannot rule out the possibility that the surface temperature is lower and the spins have not fully thermalized, but then to have measured a polarization consistent with 0.37 K and for two different molecules seems an unlikely coincidence. We also mention that eq 12 relies on the knowledge of $A_\Pi$; if more accurate values for $K_2$ and $Rb_2$ should become available, our values of $P_1 - P_3$ and $T$ will have to be rescaled accordingly. The values we used for $A_\pi$ are reported at the end of section III.D.

*2. Simulation of the Spectra.* Underneath the moment analysis lies the assumption of a crystal field splitting, although in the end the CF parameter does not appear in eq 12. As a further

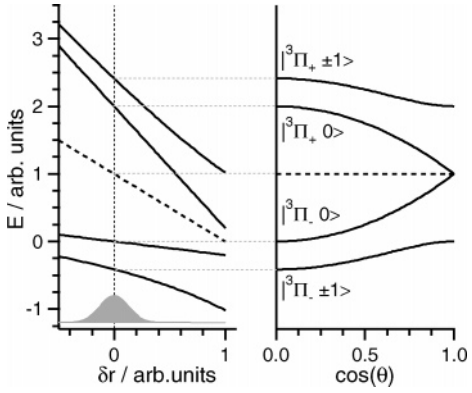


**Figure 4.** Correlation diagram for a $^3\Pi$ multiplet under the combined effect of a spin−orbit interaction and a crystal field interaction dependent on displacement from an equilibrium position $\delta r$ and molecule−surface angle $\theta$: left panel, CF interaction varies linearly with $\delta r$ at $\theta = 0$; right panel, CF splitting varies as $(1 - \cos^2 \theta)$ at $\delta r = 0$. The gray Gaussian schematizes the probability distribution of $\delta r$. The dashed line is the center of gravity of the multiplet.

test that the proposed level structure is reasonable for the $Rb_2$ $(1)^3\Pi$ manifold on a He droplet, we look at how well it accounts for the experimental LIF and MCD spectra. In doing so, we neglect the $\mathscr{A}$- and $\mathscr{B}$-type contributions to the MCD spectrum (related to magnetic-induced mixing in the excited state and to Zeeman shifts, respectively), and we only consider $\mathscr{C}$-type contributions (related to the populations of the Zeeman levels of the ground-state manifold; for a more detailed physical picture, see ref 57).

Assuming that for an ensemble of doped droplets the internuclear axis of the $Rb_2$ molecule is randomly oriented relative to the magnetic field, the spectra can be calculated, within an overall scaling factor, with eqs 23 and 25 of ref 57 (the spin temperature is set to 0.37 K). We note that as explicitly shown in Table 7 of ref 57, the two inner bands in the correlation diagram contribute to the LIF but not to the MCD spectrum. The two outer ones contribute to both: additively to the LIF and subtractively to the MCD spectrum. Furthermore, the MCD intensities depend on $\kappa = A_\Pi/V_1$ and thus on the CF-splitting $V_0$. For the molecule on the droplet, $V_0$ will depend on the distance of the molecule from the droplet, as well as on the angle $\theta$ between the internuclear axis and the droplet surface. To keep the number of free parameters small, we model the former in the most simple way. First, we assume the probability to find the molecule at a given displacement $\delta r$ from the equilibrium distance to be Gaussian. Furthermore, we assume $\bar{V}$ and $V_0$ to be linear functions of $\delta r$ (Figure 4, left panel). Hence the probability distributions of $\bar{V}(\delta r)$ and $V_0(\delta r)$ are also Gaussian. Our free parameters are their mean values, $\bar{V}(0)$, $V_0(0)$, and widths, $\bar{\sigma}$, $\sigma_0$. Symmetry arguments dictate that a Legendre polynomial expansion of $V_0(\delta r)$ to second order in $\cos\theta$ must have the form $V_0(\delta r)_{|\theta=\pi/2}(1 - \cos^2\theta)$, resulting in the correlation diagram of Figure 4, right panel. $\bar{V}(\delta r)$ should have the form $\bar{V}(\delta r)_{|\theta=\pi/2} + [\bar{V}_{|\theta=0}(\delta r) - \bar{V}(\delta r)_{|\theta=\pi/2}] \cos^2\theta$; to avoid introducing another free parameter, we only keep its average value $[\bar{V}(\delta r)_{|\theta=0} + 2\bar{V}(\delta r)_{|\theta=\pi/2}]/3$, which practically means that $\bar{V}$ and $\bar{\sigma}$ do not depend on $\theta$. We account for the vibrational structure of the $Rb_2$ molecule by convoluting the resulting spectrum with a Gaussian profile, of width $\sigma_{FCF}$, which was fitted to the calculated Franck−Condon profile of the transition. While the values of $\sigma_{FCF}$, $\bar{\sigma}$, and $\sigma_0$ are reasonable, they are also strongly correlated; thus at this point their physical significance should be taken with caution. The simulation parameters have been "hand-tuned", and their chosen values

**TABLE 1: Estimates of $V_0(0)_{|\theta=\pi/2}$ from Atomic ($\Delta V'/2$) and Molecular ($V_0^M$) Spectra and Values of Atomic ($A_P$) and Molecular ($A_\Pi$) Spin−Orbit Constants (See Section III.D) and the Remaining Parameters of the Simulations[a]**

| | $A_P$ | $A_\Pi$ | $(\Delta V'/2)$ | $V_0^M$ | $\bar{V}(0)$ | $\sigma_{FCF}$ | $\bar{\sigma}$ | $\sigma_0$ |
|---|---|---|---|---|---|---|---|---|
| $K_2$ | 19 | 19 | 55 | 55 | 13947 | 14 | 26 | 26 |
| $Rb_2$ | 79 | 70 | 100 | 65 | 13517 | 21 | 24 | 21 |
| KRb | | 38.5 | 55−100 | 60 | | | | |
| $Cs_2$ | 185 | 157 | 220 | | | | | |

[a] All values in $cm^{-1}$.

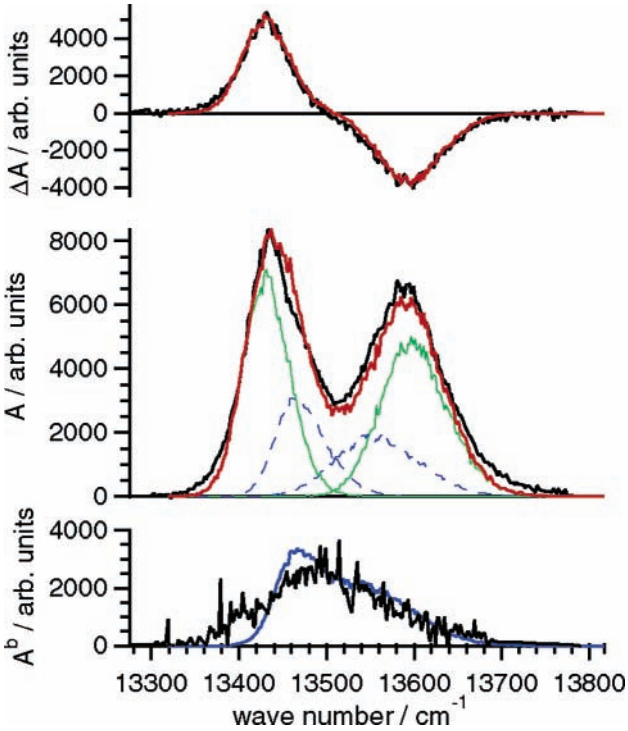


**Figure 5.** Comparison between measured (black traces) and simulated (color traces) spectra of $Rb_2$: top panel, MCD spectrum; middle panel, LIF spectrum (green solid lines are the contibutions from $|^3\Pi_\pm \pm 1\rangle$ and blue dashed lines those from $|^3\Pi_\pm 0\rangle$; the red line is their sum); bottom panel, blue-filtered LIF spectrum $A^b$ and sum of the $|^3\Pi_\pm 0\rangle$ contributions. Scaling of the simulated total spectra is arbitrary but the same for MCD and LIF.

are reported in Table 1. For convenience, the value of $\bar{V}(0)$ used in the simulation and reported in Table 1 is measured from $v = 0$, $j = 0$ of the ground state. The results of the simulation are shown in Figure 5. They match the experimental LIF and MCD spectra quite well, considering the simplicity of the model. More importantly, they allow the separation of contributions from the four CF−SO split states and predict that absorption related to the $|\Omega| = 1$ multiplet be present but unresolved. In our previous work,[34] no fluorescence from $|\Omega| = 1$ was detected, and the doubt remained whether or not $|\Omega| = 1$ was accessed in excitation. Our present data answer a "yes" to that question but leave the question open why no fluorescence from $|\Omega| = 1$ is detected in emission. In our previous work,[34] we observed that all reasonably possible emission channels (direct emission, $\Omega$-relaxation, dissociation, spin-conversion) are actually open, but we have not quantified the branching ratios as a function of excitation frequency. Here we consider the possibility of a correlation between $|\Omega| = 1$ and spin relaxation to a singlet state [note that the spin part of the wavefunction with $\Omega = \pm 1$ $(|\uparrow\downarrow\rangle + |\downarrow\uparrow\rangle)$ differs from that of a singlet state $(|\uparrow\downarrow\rangle - |\downarrow\uparrow\rangle)$ only by a phase factor]. We measured a filtered-LIF excitation spectrum (filter BG39) where only fluorescence with higher

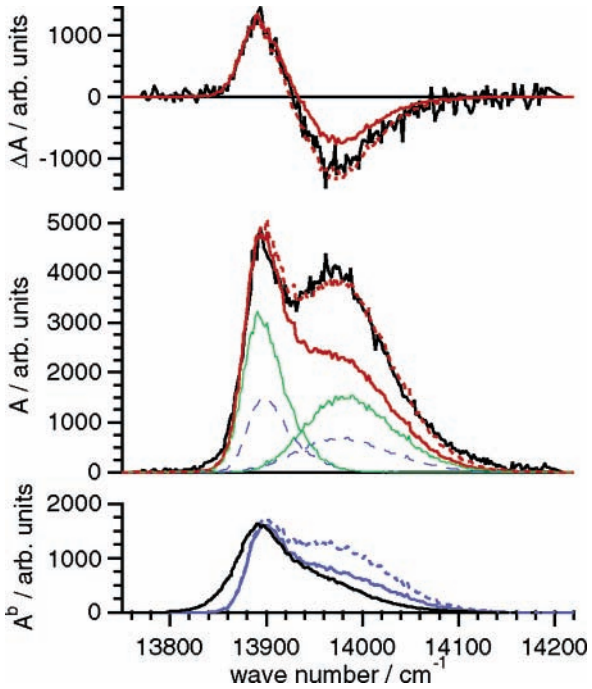


**Figure 6.** Same as Figure 5 for $K_2$. Red and blue solid lines are the normal simulation. Red and blue dashed lines are those after scaling the two rightmost contributions (from $|^3\Pi_+ 0\rangle$, $|^3\Pi_+ \pm 1\rangle$) by a factor 1.7. Blue-filtered LIF spectrum digitized from ref 52.

photon energy than the excitation laser is collected, that is, emission from the singlet manifold. The corresponding spectrum (Figure 5) is very weak (indeed blue fluorescence was not observed when dispersing emission with a spectrograph),[34] indicating that branching ratio to this channel must be small, and that the emission pathway of $|\Omega| = 1$ must be via dissociation or relaxation to $\Omega = 0$. It is interesting, however, to observe that the *shape* of the blue-filtered LIF spectrum is close to that of the contribution we predict from $\Omega = \pm 1$ (Figure 5, bottom panel).

The same observations hold for $K_2$ (Figure 6). Both LIF and MCD spectra are well reproduced, and all four components of the multiplet are present. Again, the blue-filtered LIF spectrum (whose branching ratio, incidentally, is much higher than for $Rb_2$[52]) matches well the contribution we predict from $\Omega = \pm 1$. Note however that a perfect match is only obtained if the two rightmost contributions (from $|^3\Pi_+ 0\rangle$, $|^3\Pi_+ \pm 1\rangle$) are arbitrarily scaled by a factor 1.7; at the moment, we cannot explain this discrepancy.

**D. Relation to the $^2$P State and $^2$P ← $^2$S Spectrum of an Alkali Atom on a He Droplet.** As a further test that our model is physically meaningful, we compare the CF parameter with the interaction strength of an alkali atom on a He droplet, for which experimental data[54,63,64] and a reasonable model,[63] sometimes referred to as "pseudo-diatomic", are available. In this model, one defines a reference system $x'$, $y'$, $z'$ (we use primed coordinates, to distinguish it from the one used so far) with the quantization axis $z'$ joining the center of mass of the atom and that of the droplet. A p-state alkali atom is described by its three degenerate orbitals $p^{x'}$, $p^{y'}$, $p^{z'}$. The droplet perturbation partly lifts this degeneracy such that $p^{z'}$ (perpendicular to the droplet surface) is higher in energy than $p^{x'}$ and $p^{y'}$ (parallel to the droplet surface) by an amount $\Delta V'$. SO-coupling ($A_P$) fully removes the degeneracy: one finds three eigenstates,[63] and the separation between the states with lowest and highest energy is given by $(\Delta V'^2 - 2\Delta V' A_P + 9A_P^2)^{1/2}$. Identifying the three peaks observed in experimental spectra with the energies of the corresponding eigenstates thus allows an estimate of the mean value of $\Delta V'$.

To relate the pictures of the atom- and molecule-doped droplet, we approximate the molecular orbitals $(\sigma_g)(\pi_g^{x,y})$ as a linear combination of atomic orbitals:

$$(\sigma_g)(\pi_g^{x,y}) \approx \frac{1}{\sqrt{2}}[(s_1)(p_2^{x,y}) + (s_2)(p_1^{x,y})] \qquad (13)$$

Here the subscripts 1 and 2 label the Rb atoms. If we restrict ourselves to the configuration where the molecule lies flat on the droplet (and $z'$ coincides with $x$), a direct correspondence can be made between orbitals in the primed and unprimed system, and the energy separation between $p^x$ and $p^y$ is thus $\Delta V'$. From eq 13, one sees that under the above assumptions, and the further assumptions that (i) the overlap integral between the summands of eq 13 be small and (ii) the He-density distribution for the atom- and molecule-doped droplet do not differ too much; half the atomic splitting $\Delta V'/2$ is a reasonable estimate of $V_0$. Indeed the atomic and molecular estimates summarized in Table 1 are reasonably close.

Assumption (i) is reasonable, since the $^3\Sigma_u$ ground state from which the molecule is excited has its equilibrium internuclear distance at ~6 Å. Assumption (ii) is reasonable for the coarse estimate we make here; however it is certainly a point to be improved in a more exact treatment.

We summarize the definitions and sources of the parameters reported in Table 1. $\Delta V'/2$ is estimated from atomic spectra, as just explained, and $V_0^M$ from molecular spectra. When available, that is, for $K_2$ and $Rb_2$, $V_0^M$ is the value from our simulation. For KRb, it is calculated from the peak separation $\Delta E$ in the LIF spectrum published in ref 34 by the formula $V_0^M = {}^3/_2[A_\Pi^2 - (\Delta E/2)^2]^{1/2}$. For $Cs_2$ an estimate from the LIF spectrum[54] is not possible without a full simulation since $V_0^M/A_\Pi$ seems to be too small for a reliable estimate from the peak separations.

For $Rb_2$ and KRb, $A_\Pi$ is the molecular SO constant determined from our dispersed emission spectra.[34] For $Cs_2$, it is the separation between the Franck−Condon bands calculated in ref 54. For the other molecules, we used $A_\Pi = A_P$ where $A_P$ is the atomic SO constant in the lowest $^2$P state.

## IV. Conclusions

We have simultaneously measured the LIF and MCD spectra of the $(1)^3\Pi_g \leftarrow a^3\Sigma_u$ transition for $Rb_2$ on helium nanodroplets. We present a detailed analysis of the spectra (and of those previously measured for $K_2$) based on a molecular Hamiltonian containing spin−orbit coupling $A_\Pi$ and a "crystal field" interaction $V_0$ with the droplet.

The LIF spectra show a two-peak structure, in contrast to the three peaks expected from a free-molecule Hamiltonian. Accounting for the CF-splitting of the $^3\Pi$ state explains the two-peak structure in the LIF spectrum of $K_2$, KRb, and $Rb_2$ and correctly reproduces the MCD spectra. It further predicts that the "missing" peak is split and broadened and thus hidden in the observed spectrum; fluorescence analysis suggests a correlation between this excitation peak and a singlet-state emission channel. Our approach may be able to rationalize similar structures observed in the LIF spectra of LiCs, NaCs, and $Cs_2$; in this case, inclusion of nearby electronic states is necessary. We anticipate that MCD spectra of these molecules will be very informative and possibly revealing of a more complex structure.

From the MCD spectrum of $Rb_2$, we deduce a spin temperature in agreement with the corresponding analysis for $K_2$ [15] and with the accepted temperature, 0.37 K, of the interior of a He droplet. These dimers provide the first instance of a "surface thermometer". Our data indicate that the spins have thermalized and further that the surface temperature is the same as the interior temperature.

**Acknowledgment.** We thank Lorenz Windholz, Christian Neureiter, and Olivier Allard for assistance, and Timothy C. Steimle for discussions and for carefully reading the manuscript. This research is supported by the Austrian Science Fund (FWF) under Grant P18053-N02.

## References and Notes

(1) Choi, M. Y.; Douberly, G. E.; Falconer, T.; Lewis, W. K.; Lindsay, C. M.; Merritt, J. M.; Stiles, P.; Miller, R. E. *Int. Rev. Phys. Chem.* **2006**, *25*, 15.
(2) Stienkemeier, F.; Lehmann, K. K. *J. Phys. B* **2006**, *39*, R127.
(3) Barranco, M.; Guardiola, R.; Hernandez, S.; Mayol, R.; Navarro, J.; Pi, M. *J. Low Temp. Phys.* **2006**, *142*, 1.
(4) Toennies, J. P.; Vilesov, A. F. *Angew. Chem., Int. Ed.* **2004**, *43*, 2622.
(5) *J. Chem. Phys.* **2001**, *115* (22), Special issue on Helium Nanodroplets.
(6) Brink, D.; Stringari, S. *Z. Phys. D* **1990**, *15*, 257.
(7) Hartmann, M.; Miller, R. E.; Toennies, J. P.; Vilesov, A. *Phys. Rev. Lett.* **1995**, *75*, 1566.
(8) Grebenev, S.; Toennies, J. P.; Vilesov, A. F. *Science* **1998**, *279*, 2083.
(9) Lehnig, R.; Slenczka, A. *J. Chem. Phys.* **2004**, *120*, 5064.
(10) Nauta, K.; Miller, R. E. *J. Chem. Phys.* **2001**, *115*, 4508.
(11) Nauta, K.; Miller, R. E. *J. Chem. Phys.* **2000**, *113*, 9466.
(12) Nauta, K.; Miller, R. E. *J. Chem. Phys.* **2001**, *115*, 8384.
(13) Harms, J.; Hartmann, M.; Sartakov, S.; Toennies, J. P.; Vilesov, A. *J. Mol. Spectrosc.* **1997**, *185*, 204.
(14) von Haeften, K.; Metzelthin, A.; Rudolph, S.; Staemmler, V.; Havenith, M. *Phys. Rev. Lett.* **2005**, *95*, 215301.
(15) Nagl, J.; Auböck, G.; Callegari, C.; Ernst, W. E. *Phys. Rev. Lett.* **2007**, *98*, 075301.
(16) McKellar, A. R. W.; Xu, Y. J.; Jager, W. *Phys. Rev. Lett.* **2006**, *97*, 183401.
(17) Dong, F.; Miller, R. E. *Science* **2002**, *298*, 1227.
(18) Kupper, J.; Merritt, J. M.; Miller, R. E. *J. Chem. Phys.* **2002**, *117*, 647.
(19) Higgins, J.; Ernst, W. E.; Callegari, C.; Reho, J.; Lehmann, K. K.; Gutowski, M.; Scoles, G. *Phys. Rev. Lett.* **1996**, *77*, 4532.
(20) Nauta, K.; Miller, R. E. *Science* **1999**, *283*, 1895.
(21) Nauta, K.; Moore, D. T.; Stiles, P. L.; Miller, R. E. *Science* **2001**, *292*, 481.
(22) Douberly, G. E.; Merritt, J. M.; Miller, R. E. *Phys. Chem. Chem. Phys.* **2005**, *7*, 463.
(23) Higgins, J.; Callegari, C.; Reho, J.; Stienkemeier, F.; Ernst, W. E.; Lehmann, K. K.; Gutowski, M.; Scoles, G. *Science* **1996**, *273*, 629.
(24) Lugovoj, E.; Toennies, J. P.; Vilesov, A. *J. Chem. Phys.* **2000**, *112*, 8217.
(25) *J. Phys. B* **2006**, *39* (19), Special issue on Cold Molecules.
(26) Goyal, S.; Schutt, D. L.; Scoles, G. *Phys. Rev. Lett.* **1992**, *69*, 933.
(27) Miller, R. E. *Faraday Discuss.* **2001**, *118*, 1.
(28) Higgins, J. P.; Reho, J.; Stienkemeier, F.; Ernst, W. E.; Lehmann, K. K.; Scoles, G. In *Atomic and molecular beams: the state of the art 2000*; Campargue, R., Ed.; Springer: Berlin, New York, 2001; p 723.
(29) Brühl, F. R.; Miron, R. A.; Ernst, W. E. *J. Chem. Phys.* **2001**, *115*, 10275.
(30) Mudrich, N.; Bunermann, O.; Stienkemeier, F.; Dulieu, O.; Weidemuller, M. *Eur. Phys. J. D* **2004**, *31*, 291.
(31) Ernst, W. E.; Huber, R.; Jiang, S.; Beuc, R.; Movre, M.; Pichler, G. J. *Chem. Phys.* **2006**, *124*, 024313.
(32) Przystawik, A.; Radcliffe, P.; Gode, S. G.; Meiwes-Broer, K. H.; Tiggesbäumker, J. *J. Phys. B* **2006**, *39*, S1183.
(33) Higgins, J.; Hollebeek, T.; Reho, J.; Ho, T.-S.; Lehmann, K. K.; Rabitz, H.; Scoles, G. *J. Chem. Phys.* **2000**, *112*, 5751.
(34) Allard, O.; Nagl, J.; Auböck, G.; Callegari, C.; Ernst, W. E. *J. Phys. B* **2006**, *39*, S1169.
(35) Hartmann, M.; Mielke, F.; Toennies, J. P.; Vilesov, A. F.; Benedek, G. *Phys. Rev. Lett.* **1996**, *76*, 4560.
(36) Reho, J.; Higgins, J.; Callegari, C.; Lehmann, K. K.; Scoles, G. *J. Chem. Phys.* **2000**, *113*, 9686.
(37) Reho, J.; Higgins, J.; Lehmann, K. K.; Scoles, G. *J. Chem. Phys.* **2000**, *113*, 9694.
(38) Federmann, F.; Hoffmann, K.; Quaas, N.; Close, J. D. *Phys. Rev. Lett.* **1999**, *83*, 2548−2551.
(39) Stienkemeier, F.; Meier, F.; Hägele, A.; Lutz, H. O.; Schreiber, E.; Schulz, C. P.; Hertel, I. V. *Phys. Rev. Lett.* **1999**, *83*, 2320.
(40) Schulz, C.; Claas, P.; Stienkemeier, F. *Phys. Rev. Lett.* **2001**, *87*, 153401.
(41) Droppelmann, G.; Bunermann, O.; Schulz, C. P.; Stienkemeier, F. *Phys. Rev. Lett.* **2004**, *93*, 23402.
(42) Doppner, T.; Fennel, T.; Diederich, T.; Tiggesbäumker, J.; Meiwes-Broer, K. H. *Phys. Rev. Lett.* **2005**, *94*, 013401.
(43) Higgins, J.; Callegari, C.; Reho, J.; Stienkemeier, F.; Ernst, W. E.; Gutowski, M.; Scoles, G. *J. Phys. Chem. A* **1998**, *102*, 4952.
(44) Stienkemeier, F.; Meier, F.; Lutz, H. O. *J. Chem. Phys.* **1997**, *107*, 10816.
(45) Stienkemeier, F.; Meier, F.; Lutz, H. O. *Eur. Phys. J. D* **1999**, *9*, 313.
(46) Hartmann, M.; Lindinger, A.; Toennies, J. P.; Vilesov, A. F. *Chem. Phys.* **1998**, *239*, 139.
(47) Hartmann, M.; Lindinger, A.; Toennies, J. P.; Vilesov, A. F. *J. Phys. Chem. A* **2001**, *105*, 6369.
(48) Lindinger, A.; Lugovoj, E.; Toennies, J. P.; Vilesov, A. F. *Z. Phys. Chem.−Int. J. Res. Phys. Chem. Chem. Phys.* **2001**, *215*, 401.
(49) Lehnig, R.; Slenczka, A. *J. Chem. Phys.* **2003**, *118*, 8256.
(50) Lehnig, R.; Slipchenko, M.; Kuma, S.; Momose, T.; Sartakov, B.; Vilesov, A. *J. Chem. Phys.* **2004**, *121*, 9396.
(51) Lehnig, R.; Slenczka, A. *J. Chem. Phys.* **2005**, *122*, 244317.
(52) Reho, J. H.; Higgins, J. P.; Lehmann, K. K. *Faraday Discuss.* **2001**, *118*, 33.
(53) Reho, J. H.; Higgins, J.; Nooijen, M.; Lehmann, K. K.; Scoles, G.; Gutowski, M. *J. Chem. Phys.* **2001**, *115*, 10265.
(54) Bünermann, O.; Mudrich, M.; Weidemüller, M.; Stienkemeier, F. *J. Chem. Phys.* **2004**, *121*, 8880.
(55) Ralchenko, Yu.; Jou, F.-C.; Kelleher, D. E.; Kramida, A. E.; Musgrove, A.; Reader, J.; Wiese, W. L.; Olsen, K. *NIST Atomic Spectra Database* (version 3.1.1); National Institute of Standards and Technology: Gaithersburg, MD, 2007; available online at http://physics.nist.gov/asd3 [2007, March 26].
(56) Kotochigova, S.; Tiesinga, E.; Julienne, P. S. *Phys. Rev. A* **2000**, *63*, 012517.
(57) Langford, V. S.; Williamson, B. E. *J. Phys. Chem. A* **1998**, *102*, 2415.
(58) Mills, P. D. A.; Western, C. M.; Howard, B. J. *J. Phys. Chem.* **1986**, *90*, 3331.
(59) Fawzy, W. M.; Hougen, J. T. *J. Mol. Spectrosc.* **1989**, *137*, 154.
(60) Dubernet, M.-L.; Flower, D.; Hutson, J. M. *J. Chem. Phys.* **1991**, *94*, 7602.
(61) Marshall, M. D.; Lester, M. I. *J. Chem. Phys.* **2004**, *121*, 3019.
(62) We have measured beam depletion spectra, which have a worse signal to noise ratio but essentially match LIF spectra. This supports the validity of the assumption. Because several fluorescence emission channels, at different wavelengths, are possible[34] a very accurate quantitative treatment may require corrections due to the response of the photomultiplier.
(63) Stienkemeier, F.; Higgins, J.; Callegari, C.; Kanorsky, S. I.; Ernst, W. E.; Scoles, G. *Z. Phys. D* **1996**, *38*, 253.
(64) Brühl, F. R.; Trasca, R. A.; Ernst, W. E. *J. Chem. Phys.* **2001**, *115*, 10220.